ELSEVIER

Journal of Fluids and Structures 24 (2008) 1077–1097

JOURNAL OF FLUIDS AND STRUCTURES

www.elsevier.com/locate/jfs

Interaction between a submerged evacuated cylindrical shell and a shock wave—Part I: Diffraction–radiation analysis

S. Iakovlev

Department of Engineering Mathematics and Internetworking, Dalhousie University, Halifax, NS, Canada B3J 2X4

Received 27 June 2006; accepted 28 January 2008
Available online 18 April 2008

Abstract

The interaction between a submerged elastic circular cylindrical shell and an external shock wave is addressed. A linear, two-dimensional formulation of the problem is considered. A semi-analytical solution is obtained using a combination of the classical analytical approach based on the use of the Laplace transform and separation of variables, and finite difference methodology. The study consists of two parts. Part I focuses on the simulation and analysis of the acoustic fields induced during the interaction. Both the diffraction (absolutely rigid cylinder) and complete diffraction–radiation (elastic shell) are considered. Special attention is paid to the lower-magnitude shell-induced waves representing radiation by the elastic waves circumnavigating the shell. The focus of Part II is on the numerical analysis of the solution. The convergence of the series solution and finite-difference scheme is analysed. The computation of the response functions of the problem is discussed as well, as is the effect of the bending stiffness on the acoustic field. The membrane model of the shell is considered to analyse such an effect, which, in combination with the models addressed in Part I, allows for the analysis of the evolution of the acoustic field around the structure as its elastic properties change from an absolutely rigid cylinder to a membrane. The results of the numerical simulations are compared to available experimental data, and a good agreement is observed.

1. Introduction

Submerged evacuated shells subjected to an external shock wave are, perhaps, the most extensively studied shock-interacting engineering structures. A long-term and well-funded interest of the navies world-wide in underwater explosions and their effect on ships, submersible vehicles, and other offshore structures has been the main reason for this area of the fluid–structure interaction research to advance more rapidly than others. As a result, the many aspects of this complex phenomena have been addressed, some better than others, and extensive data was produced to answer many practical questions necessary to advance marine structures.

The present paper offers another look at the interaction between an empty circular cylindrical shell and a shock wave propagating in the external fluid. A linear model is employed to simulate the interaction, and both the structural and fluid dynamics are addressed. Considering the abundant and diverse literature published on the topic, it may appear that yet another study, especially one that employs a linear model with its inherent limitations, is not a priority. However, in the author's opinion, such a study is worth undertaking for a number of reasons.

E-mail address: serguei.iakovlev@dal.ca

0889-9746/$ - see front matter © 2008 Elsevier Ltd. All rights reserved.
doi:10.1016/j.jfluidstructs.2008.01.004

Nomenclature

c_f	sound speed in the fluid, $\hat{c}_f = 1$
c_s	sound speed in the shell material, $\hat{c}_s = c_s c_f^{-1}$
h_0	thickness of the shell, $\hat{h}_0 = h_0 r_0^{-1}$
K_n	modified Bessel function of the second kind of order n
p_α	peak incident pressure, $\hat{p}_\alpha = p_\alpha \rho_f^{-1} c_f^{-2}$
p	total pressure in the fluid, $\hat{p} = p \rho_f^{-1} c_f^{-2}$
p_0	incident pressure, $\hat{p}_0 = p_0 \rho_f^{-1} c_f^{-2}$
p_d	diffraction pressure, $\hat{p}_d = p_d \rho_f^{-1} c_f^{-2}$
p_r	radiation pressure, $\hat{p}_r = p_r \rho_f^{-1} c_f^{-2}$
p_s	pressure on the shell surface, $\hat{p}_s = p_s \rho_f^{-1} c_f^{-2}$
r	radial coordinate of the polar coordinate system, $r = \varrho r_0^{-1}$
r_0	radius of the shell, $\hat{r}_0 = 1$
R_0	radial distance to the source of the incident wave, $\hat{R}_0 = R_0 r_0^{-1}$
S_R	incident shock wave stand-off, $\hat{S}_R = S_R r_0^{-1}$
t	time, $t = \tau c_f r_0^{-1}$
v^*	transverse displacement of the middle surface of the shell, $v = v^* r_0^{-1}$
w^*	normal displacement of the middle surface of the shell, $w = w^* r_0^{-1}$
ε	strain in the middle surface of the shell
θ	angular coordinate of the polar coordinate system
λ	exponential decay rate, $\hat{\lambda} = \lambda c_f r_0^{-1}$
ν	Poisson's ratio
ξ_n^e	'volume' response functions
ρ_f	density of the fluid, $\rho_f = 1$
ρ_s	density of the shell material, $\hat{\rho}_s = \rho_s \rho_f^{-1}$
ϱ	radial coordinate of the polar coordinate system, $r = \varrho r_0^{-1}$
τ	time, $t = \tau c_f r_0^{-1}$
ϕ	total fluid velocity potential, $\hat{\phi} = \phi c_f^{-1} r_0^{-1}$
ϕ_0	fluid velocity potential in the incident wave, $\hat{\phi}_0 = \phi_0 c_f^{-1} r_0^{-1}$
ϕ_d	fluid velocity potential in the diffracted wave, $\hat{\phi}_d = \phi_d c_f^{-1} r_0^{-1}$
ϕ_r	fluid velocity potential in the radiated wave, $\hat{\phi}_r = \phi_r c_f^{-1} r_0^{-1}$
ψ_n^e	'surface' response functions
$(*)_n \sin n\theta$ and $(*)_n \cos n\theta$	denote the harmonics of (*). Unless stated otherwise, capitalized symbols denote the Laplace transforms of the corresponding functions. Other symbols are defined in the text

First, the linear model employed in the present work has recently been used by the author to simulate the interaction between a shock wave and a fluid-filled submerged shell (Iakovlev, 2006, 2007). Among other assumptions, it was assumed that the external and internal fluids have identical properties. Such an assumption allowed for concentrating on the multitude of wave reflection phenomena without a need to address the effects present due to the difference in the properties of the fluids at the same time. Unfortunately, it also meant that the most intriguing case of two different fluids had to be left for future investigation.

In order to approach the two-fluid problem, the internal and external fields will have to be considered simultaneously, i.e. a complete internal–external analysis of the interaction will have to be carried out. To accomplish that, along with the available solution for the internal field, a matching (i.e. obtained using the same linear methodology) solution for the external field will be needed as well. Therefore, solving the external problem is a necessary step before the case of two different fluids can be approached. Such a solution, to the best of the author's knowledge, has not yet been developed.

Second, comparing the results produced by a linear model to experimental data will allow for verification of the solution developed. More importantly, it will also allow for analysis of the limitations of the linear model as it applies to the interaction between shells and a specific class of shock loads (weak shock waves and acoustic pulses). Such analysis, coupled with that of the interaction between the shell and a shock wave in the context of the internal fluid (Iakovlev, 2006, 2007), will allow for a confident use of the present model to simulate the dynamics of more complex shell systems experiencing shock loads of similar nature.

Furthermore, converged analytical solutions used as benchmarks seem to be quite popular amongst the underwater explosion community [e.g., Mair (1999b)]. To that end, if the linear model employed proves to be adequate, another converged analytical solution will be added to a series of solutions that the author set to develop (Iakovlev, 2006) for possible use as benchmarks. The solution will also be suitable for verification of both structural dynamics codes and those intended for analysis of the pressure fields induced during the interaction.

Third, it will be possible to study in detail the dynamics of the external pressure field, including both the scattered and shell-radiated components. Such analysis will allow for a much better understanding of the dynamics of the interaction between shock waves and elastic structures. For example, even though the radiated pressure is known to significantly change the resulting shock load on the structure, clarifying its contribution into the total acoustic field, both in terms of

its magnitudes and the geometry of the radiated field, certainly appears to be of interest. Sequential images of the external field will also be an informative complement to the many existing studies of the stress–strain states of shock-subjected cylindrical shells.

The analysis of the external field will allow one to address a number of secondary issues of practical interest as well. One of the possible issues is considering a scenario where secondary structures are placed around the primary cylindrical shell. If the geometry of those is such that they do not significantly change the acoustic fields induced by the primary structure (e.g., cables, small pipes, auxiliary equipment, etc.), then it is reasonable to expect that the model employed can be successfully used to estimate the shock loading that such secondary structures would experience in the wake of the response of the primary one to a shock wave.

In order to put the present work in the context of the literature published on shell–shock interaction, we mention some of the papers devoted to various aspects of the problem, and emphasize what is new in the present study. A much more comprehensive literature review can be found in Iakovlev (2006).

Even though the diffraction represents only one aspect of the interaction between elastic shells and shocks, it certainly is an interesting problem on its own, and a large number of studies were devoted to the diffraction of shock waves on rigid cylinders. Bryson and Gross (1961) presented experimental images of the diffraction on cylinders, as did Heilig, W.H. (1969), Heilig, G. (1999) and Oakley et al. (1999). Numerical investigation of the diffraction pressure fields was carried out, for example, by Yang and Liu (1987), Ofengeim and Drikakis (1997), Drikakis et al. (1997), Sun (1998), and Heilig (1999). A number of earlier publications addressed the surface distribution of the diffraction pressure, mostly using analytical solutions of the respective linear problems [e.g., Geers (1972), Huang and Wang (1971); some of the numerical works mentioned presented time-histories of the surface pressure as well]. It appears, however, that the diffraction *field* around a shock-interacting shell has not yet been addressed using an *analytical* solution. The present paper fills this gap.

A number of publications addressed the interaction between acoustic pulses and shells (or elastic bodies) experimentally, with the focus on the various waves radiated by the structure. Neubauer and Dragonette (1970), as well as Neubauer (1968a,b) studied various types of waves radiated by a cylinder and cylindrical shells of various thicknesses, but considered mostly partial insonification or angular incidence. Ahyi et al. (1998) addressed a variety of waves radiated by a shell subjected a very short symmetric acoustic pulse, but only considered the very early interaction, prior to the instant when the incident wave passed over the shell. Merlen et al. (1995) and Latard et al. (1999) visualized the interaction of an acoustic pulse and an elastic spherical body, and Takano et al. (1997) considered the radiation by an elastic cylindrical body. It seems, however, that the fully developed shell-radiated wave system (i.e. the radiated field observed after the elastic waves have propagated around the shell several times) was not addressed for the case of a symmetric insonification of the entire shell. Analysis of the fully developed radiation [images similar to figures 1 and 2 of Neubauer and Dragonette (1970)] certainly appears to be of interest, and is another goal of the present paper.

A rather limited number of studies were devoted to the numerical simulation of the non-stationary interaction between cylindrical shells and acoustic pulses [e.g., Voinovich et al. (2001), where, amongst other simulations, the experimental images by Ahyi et al. (1998) were matched exceptionally well]. It appears, however, that a fully linear formulation of the problem adopted in the present paper (with its inherent limitations but also with the possibilities it offers in terms of obtaining an analytical solution) has not yet been used to simulate the complete diffracted–radiated field around a shock-subjected shell. As was mentioned earlier, such simulation, coupled with the comparison to experimental data, will be very helpful in determining how significant the limitations of a linear model are.

We also mention that a vast majority of the publications seem to concentrate on either rigid structures or elastic ones. This is certainly understandable since from the practical point of view, one is usually only concerned with one of the mentioned scenarios. From the theoretical point of view, however, it appears of interest to look at the 'evolution' of the acoustic field around a structure when its elastic properties change from the absolutely rigid state to the membrane one. Wardlaw and Luton (2000) discussed how the pressure changes when a rigid structure is replaced with its elastic counterpart, but considered an explosion inside a cylinder, and concentrated on non-linear effects such as cavitation. In the present work, we discuss in detail how the external field evolves when the stiffness of the structure changes. As a part of this study, the effect of the bending stiffness on the total acoustic field is discussed, and shells of different thicknesses are considered.

The publications devoted mostly or exclusively to numerical analysis of analytical solutions of shell–shock interaction problems are somewhat limited. Some of the recent contributions include studies by Zhang and Geers (1993), Huang and Mair (1996), and Sprague and Geers (1999) in which the issues pertaining to the series convergence are addressed, and various convergence improvement techniques are discussed, particularly Cesaro summation. None of the works mentioned, however, seem to address the convergence of the pressure series inside the fluid domain, and only focus on the shell surface. The present study includes the analysis of the series convergence both on the shell surface and in the surrounding fluid. Also, the analysis of the convergence of the finite-difference scheme used at the later stages of the solution is included as well.

Last but not least, the approach used here is an extension of the now classical methodology introduced and developed almost four decades ago [e.g., Geers (1969)]. Even though such methodology was extensively and successfully used over the years to analyse stress–strain states of and/or pressure distribution on the surface of shock-subjected cylindrical shells [e.g., Huang and Wang (1970), Geers (1972), Huang (1975, 1979), and Iakovlev (2004)], it seems that it has not been employed to simulate the acoustic fields around shock-interacting cylindrical shells. In the author's opinion, it certainly appears of interest to see how efficient the classical solution is and what results it produces when being extended to the case of the two-dimensional acoustic fields. Such an extension is yet another goal of the present work.

The study is divided into two parts. The problem formulation and solution, as well as most of the numerical simulations of practical interest are the subject of Part I, and Part II deals with the numerical aspects of the solution, as well as addresses the difference between the acoustic fields produced by two different shell deformation models.

2. Mathematical formulation

We consider a thin circular cylindrical shell of radius r_0 and thickness h_0. We assume that $h_0/r_0 \ll 1$ and that the deflections of the shell are small compared to its thickness, so the linear theory of thin shells is applicable. We also assume that the fibres of the shell normal to its middle surface remain so after the deformation (the Love–Kirchhoff hypothesis). The density, Poisson's ratio, and Young's modulus of and the sound speed in the shell material are ρ_s, ν, E_s, and $c_s = E^{1/2}\{\rho_s(1-\nu^2)\}^{-1/2}$, respectively. The transverse and normal displacements of the middle surface of the shell are v^* and w^*, respectively. The shell is submerged into linearly compressible, irrotational, non-viscous fluid with density ρ_s, and sound speed c_f. The shell is subjected to a step-exponential shock wave propagating in the external fluid with the decay constant λ and the pressure in the front p_α.

We consider a two-dimensional simplification of the problem, i.e. ignore the longitudinal variation of the hydrodynamic pressure and shell displacements, effectively assuming that the shell is infinitely long and is subjected to an infinitely long shock wave that has the same pressure profile in every cross-section. This is a very significant simplification, and one may question the value of the results obtained using such a model. However, in the author's opinion, the simplified model proposed is quite acceptable in the context of the present study.

Namely, it was shown (Iakovlev, 2004) that when a circular cylindrical shell is subjected to a spherical shock wave with a relatively distant source, the three-dimensional stress–strain state of the shell is dominated by the transverse stress. In the same study, it was established that the transverse stress reaches its absolute maximum in the middle cross-section of the shell (i.e. in the plane coinciding with the plane of symmetry of the incident wave). It was therefore concluded that when the extremities of the stress–strain state are the primary concern, analysing the middle cross-section is the first priority. In that light, it was tempting to introduce a simplified two-dimensional model that would only account for the middle cross-section while ignoring the rest of the shell, and hence be more computationally efficient.

Before such a simplified model could be used for analysis, it was, of course, necessary to compare the results it produced to those obtained using its three-dimensional counterpart. Such comparison was carried out in Iakovlev (2007), and the strain state in the middle cross-section of a cylindrical shell subjected to a spherical shock wave was compared to the strain state obtained using a simplified model, i.e. an infinitely long shell subjected to a shock wave without the longitudinal variation of pressure (effectively, the middle cross-section of the spherical shock wave was infinitely extended longitudinally in both directions, thus resulting in a 'cylindrical' shock wave). The two strain states were found to be very similar, and it was concluded that as far as the middle cross-section is concerned, the simplified two-dimensional model captures the most important features of the three-dimensional stress–strain state very well.

Thus, we can say with a degree of confidence that a simplified two-dimensional model is quite useful, at least when the stress–strain state is the primary concern. What about the fluid dynamics of the interaction? No explicit comparisons of the hydrodynamic fields produced by the two models have been made by the author as of yet, and only such comparison would provide a definitive answer. However, since the stress state is driven by both the fluid dynamics effects and elastic waves propagating in the shell, a good agreement in the stress–strain states suggests that the main features of the hydrodynamic fields in the middle cross-section are similar as well for the type of loading considered, i.e. a spherical shock wave with a distant source.

We also note that two-dimensional solutions have long been regarded as reliable benchmarks for the numerical modelling of the structural response to underwater explosions [see a compilation of benchmarks by Mair (1999b)], especially when it comes to more structurally advanced systems [e.g., concentric cylinders of Huang (1979)]. One of the primary goals of the present work is to develop a solution component that would eventually allow one to address the complete internal–external field for more complex shell systems, and hence the present study fits well into the big picture of the current research effort in the area. The present solution is also an extension of a definitively classical solution by Geers (1969) which is two-dimensional as well.

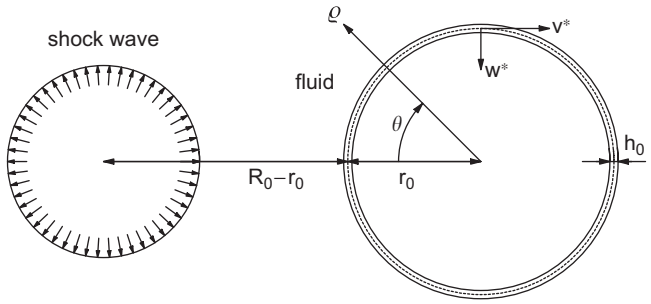

Fig. 1. Schematic of the problem (the case of a cylindrical incident wave).

One, of course, has to clearly understand the limitations of such a simplified model. For example, when the longitudinal variation of the stresses and pressure is of interest, the simplified model is of no use. The complete three-dimensional study of the interaction, however, is a more advanced stage of a system's analysis, and having a preliminary idea about the main features of the dynamics of the process at earlier design stages is still beneficial. Also, the use of the simplified model will probably become more questionable when the source of the incident wave is located closer to the shell. But in that case, the linear model itself becomes increasingly less suitable, thus it is not really an issue.

Summarizing the points made, the author believes that the present simplified model is quite useful and has its definitive niche. It can be used both as a source of estimates for the peak stresses, and, more importantly, as a source of information about the overall physics of the interaction. Furthermore, some of the systems for which the author intends to use the solution introduced here have not been addressed in the shell–shock interaction context as of yet. To that end, even qualitative results obtained by using the simplifications introduced here appear to be of considerable value.

As for the incident wave, we assume that it is either plane or cylindrical. The source of a cylindrical shock wave is located at the distance R_0 from the axis of the shell, hence the stand-off of the wave is $S_R = R_0 - r_0$. The polar coordinate system (ϱ, θ) centred on the axis of the shell is employed. The schematic of the problem for the case of a cylindrical incident wave is shown in Fig. 1; the case of a plane wave is not illustrated but the wave is assumed to propagate in the same direction (left to right), with the front being perpendicular to the line $\theta = 0$. Some issues arising when such two-dimensional incident loads are used are addressed in Appendix, along with the respective equations for the incident potential and pressure.

The fluid is governed by the wave equation

$$\nabla^2\phi = \frac{1}{c_f^2}\frac{\partial^2\phi}{\partial\tau^2}, \tag{1}$$

where ϕ is the fluid velocity potential, and τ is time (it is assumed that $\tau = 0$ corresponds to the instant when the incident wave first impinges on the shell).

Under the assumption of the Love–Kirchhoff hypothesis the shell equations in displacements are [Junger and Feit (1972, p. 237); note that since the normal displacement is considered to be positive outward in that work, and inward here, some of the terms appear in (2) and (3) with the opposite sign]

$$\frac{1}{r_0^2}\frac{\partial^2 v^*}{\partial\theta^2} - \frac{1}{r_0^2}\frac{\partial w^*}{\partial\theta} + k_0^2\left(\frac{1}{r_0^2}\frac{\partial^3 w^*}{\partial\theta^3} + \frac{1}{r_0^2}\frac{\partial^2 v^*}{\partial\theta^2}\right) = \frac{1}{c_s^2}\frac{\partial^2 v^*}{\partial\tau^2}, \tag{2}$$

$$\frac{1}{r_0^2}w^* - \frac{1}{r_0^2}\frac{\partial v^*}{\partial\theta} + k_0^2\left(\frac{1}{r_0^2}\frac{\partial^4 w^*}{\partial\theta^4} + \frac{1}{r_0^2}\frac{\partial^3 v^*}{\partial\theta^3}\right) = \chi p|_{\varrho=r_0} - \frac{1}{c_s^2}\frac{\partial^2 w^*}{\partial\tau^2}, \tag{3}$$

where $k_0^2 = h_0^2/(12r_0^2)$, $\chi = (h_0\rho_s c_s^2)^{-1}$, and p is the total pressure in the fluid. The strain in the middle surface of the shell is given by

$$\varepsilon = \frac{1}{r_0}\left(\frac{\partial v^*}{\partial\theta} - w^*\right). \tag{4}$$

The total pressure in the fluid is contributed by the incident, diffraction, and radiation pressure, p_0, p_d, and p_r, respectively,

$$p = p_0 + p_d + p_r. \tag{5}$$

The fluid velocity potential can be written as a sum of three components as well

$$\phi = \phi_0 + \phi_d + \phi_r, \tag{6}$$

where ϕ_0, ϕ_d, and ϕ_r are the potentials in the incident, diffracted, and radiated waves, respectively. We note that it often seems to be more appropriate to refer to $p_0 + p_d$ as the 'diffraction pressure', not p_d alone.

The motion of the shell is coupled to that of the fluid via the dynamic boundary condition on the interface

$$\left.\frac{\partial \phi_r}{\partial \varrho}\right|_{\varrho=r_0} = -\frac{\partial w^*}{\partial \tau}. \tag{7}$$

For the diffracted wave we have

$$\left.\frac{\partial \phi_d}{\partial \varrho}\right|_{\varrho=r_0} = -\left.\frac{\partial \phi_0}{\partial \varrho}\right|_{\varrho=r_0}. \tag{8}$$

The radiation and diffraction potentials also satisfy the zero boundary condition at the infinity

$$\phi_r \to 0 \quad \text{and} \quad \phi_d \to 0 \quad \text{when} \quad r \to \infty, \tag{9}$$

the periodicity condition with respect to the angular coordinate θ, and the zero initial conditions.

Throughout the present work, we are using the dimensionless formulation of the problem. Specifically, we normalize all variables to r_0, c_f, and ρ_f. Amongst other advantages, this allows for more convenient numerical values of the time (e.g., two dimensionless time units correspond to the time necessary for the incident wave to move over the shell of any radius, as opposed to the small respective dimensional value, in the range of 0.5–5 ms for a typical shell structure this work is concerned with). With some exceptions (the dimensionless time t, radial coordinate r, and displacements v and w), a hat is used to distinguish a dimensionless variable from its dimensional counterpart. The dimensionless fluid and shell equations are

$$\nabla^2 \hat{\phi} = \frac{\partial^2 \hat{\phi}}{\partial t^2} \tag{10}$$

and

$$\frac{\partial^2 v}{\partial \theta^2} - \frac{\partial w}{\partial \theta} + k_0^2\left(\frac{\partial^3 w}{\partial \theta^3} + \frac{\partial^2 v}{\partial \theta^2}\right) = \frac{1}{\hat{c}_s^2}\frac{\partial^2 v}{\partial t^2}, \tag{11}$$

$$w - \frac{\partial v}{\partial \theta} + k_0^2\left(\frac{\partial^4 w}{\partial \theta^4} + \frac{\partial^3 v}{\partial \theta^3}\right) = \hat{\chi}\hat{p}|_{r=1} - \frac{1}{\hat{c}_s^2}\frac{\partial^2 w}{\partial t^2}, \tag{12}$$

respectively, where $\hat{c}_s = c_s c_f^{-1}$ and $\hat{\chi} = \rho_f c_f^2 r_0 (\rho_s c_s^2 h_0)^{-1}$, which are complemented by the dimensionless boundary conditions

$$\left.\frac{\partial \hat{\phi}_r}{\partial r}\right|_{r=1} = -\frac{\partial w}{\partial t} \tag{13}$$

and

$$\left.\frac{\partial \hat{\phi}_d}{\partial r}\right|_{r=1} = -\left.\frac{\partial \hat{\phi}_0}{\partial r}\right|_{r=1}. \tag{14}$$

3. Diffraction and radiation

In order to obtain the diffraction and radiation pressure, we first apply the Laplace transform time-wise to the wave equation (10) written in the cylindrical coordinates to arrive at

$$\frac{\partial^2 \hat{\Phi}}{\partial r^2} + \frac{1}{r}\frac{\partial \hat{\Phi}}{\partial r} + \frac{1}{r^2}\frac{\partial^2 \hat{\Phi}}{\partial \theta^2} - s^2 \hat{\Phi} = 0, \tag{15}$$

where $\hat{\Phi}$ is the Laplace transform of $\hat{\phi}$, and s is the transform variable, and then separate the spatial variables to obtain the general solution of (15) satisfying the zero condition at $r = \infty$ as

$$\hat{\Phi} = A_n \mathrm{K}_n(rs)\cos n\theta, \quad n = 0, 1, \ldots, \tag{16}$$

where K_n is the modified Bessel function of the second kind of order n, and A_n is an arbitrary function of s.

If we express the normal velocity at and normal displacement of the shell surface in a series form,

$$\left.\frac{\partial \hat{\phi}_0}{\partial r}\right|_{r=1} = \sum_{n=0}^{\infty} b_n(t)\cos n\theta \tag{17}$$

and

$$w = \sum_{n=0}^{\infty} w_n(t)\cos n\theta, \tag{18}$$

respectively, and impose the boundary conditions, the Laplace transforms of the harmonics of the unknown potential components can be obtained as

$$\hat{\Phi}_n^d = B_n\ \Xi_n^e \cos n\theta \tag{19}$$

and

$$\hat{\Phi}_n^r = sW_n\ \Xi_n^e \cos n\theta, \tag{20}$$

where B_n and W_n are the Laplace transforms of b_n and w_n, respectively, and Ξ_n^e are the Laplace transforms of the response functions of the problem ξ_n^e,

$$\Xi_n^e(r, s) = -\frac{\mathrm{K}_n(rs)}{s\mathrm{K}_n'(s)}. \tag{21}$$

The response functions represent the response of the external fluid to the motion of the shell surface and/or to the scattering of waves by the shell. They do not depend on the parameters of the shell and are completely determined by the geometry of the problem. The latter feature makes an approach based on the use of the response functions very attractive from the computational point of view—once they have been computed sufficiently accurately, the interaction can be easily simulated for any incident wave and any cylindrical shell.

The functions ξ_n^e represent the response anywhere in the fluid, and it is therefore appropriate to refer to them as the 'volume' response functions, as opposed to the 'surface' ones that only represent the response of the fluid in the immediate contact with the shell. The 'surface' response functions for the present geometry, ψ_n^e, were addressed earlier [e.g., Iakovlev (2004)], and their Laplace transforms are given by

$$\Psi_n^e(s) = -\frac{\mathrm{K}_n(s)}{s\mathrm{K}_n'(s)}. \tag{22}$$

The 'volume' response functions can be easily reduced to their 'surface' counterparts by setting $r = 1$,

$$\xi_n^e(1, t) = \psi_n^e(t). \tag{23}$$

Taking into account that for the pressure p and fluid velocity potential ϕ we have

$$p = -\rho_f \frac{\partial \phi}{\partial \tau}\left[\text{or } \hat{p} = -\frac{\partial \hat{\phi}}{\partial t} \text{ in the dimensionless form}\right], \tag{24}$$

and applying some theorems related to the Laplace transform to (19) and (20), we obtain the diffraction and radiation pressure as

$$\hat{p}_d = \sum_{n=0}^{\infty} \hat{p}_n^d \cos n\theta \tag{25}$$

and

$$\hat{p}_r = \sum_{n=0}^{\infty} \hat{p}_n^r \cos n\theta, \tag{26}$$

where

$$\hat{p}_n^d = -\frac{1}{\sqrt{r}}\, b_n(t) - \int_0^t b_n(\eta)\, \frac{\mathrm{d}\xi_n^e}{\mathrm{d}\eta}(r, t-\eta)\, \mathrm{d}\eta \tag{27}$$

and

$$\hat{p}_n^r = -\int_0^t \frac{\mathrm{d}^2 w_n(\eta)}{\mathrm{d}\eta^2}\, \xi_n^e(r, t-\eta)\, \mathrm{d}\eta. \tag{28}$$

Then, the total pressure in the fluid is given by

$$\hat{p} = \sum_{n=0}^{\infty} \hat{p}_n \cos n\theta, \tag{29}$$

where

$$\hat{p}_n = \hat{p}_n^d + \hat{p}_n^r + \hat{p}_n^0, \tag{30}$$

and $\hat{p}_n^0$ is given by

$$\hat{p}_0 = \sum_{n=0}^{\infty} \hat{p}_n^0 \cos n\theta. \tag{31}$$

As is apparent from (25) to (31), once the response functions ξ_n^e are known, the computation of the diffraction and radiation pressure anywhere in the fluid is reduced to implementing mostly routine numerical algorithms. Thus, the computation of the response functions is the first priority of the present study, as well as its biggest mathematical challenge. Due to the relative complexity of the procedure and a variety of associated numerical issues, it is addressed separately in Part II, along with other numerical aspects of the problem.

4. Structural dynamics

To compute the dimensionless displacements of the middle surface of the shell, v and w, we consider their series expansions

$$v = \sum_{n=0}^{\infty} v_n \sin n\theta, \quad w = \sum_{n=0}^{\infty} w_n \cos n\theta \tag{32,33}$$

and rewrite the shell equations (11) and (12) in terms of the harmonics $v_n \sin n\theta$ and $w_n \cos n\theta$. This yields, for every n, a system of two equations

$$\gamma^2 \frac{\mathrm{d}^2 v_n}{\mathrm{d}t^2} + c_n^{11} v_n + c_n^{12} w_n = 0, \tag{34}$$

$$\gamma^2 \frac{\mathrm{d}^2 w_n}{\mathrm{d}t^2} + c_n^{21} v_n + c_n^{22} w_n = \hat{\chi}\left\{\hat{p}_n^0 + \hat{p}_n^d - \int_0^t \frac{\mathrm{d}^2 w_n(\eta)}{\mathrm{d}\eta^2}\, \xi_n^e(r, t-\eta)\, \mathrm{d}\eta\right\}\Big|_{r=1}, \tag{35}$$

where

$$c_n^{11} = n^2 + k_0^2 n^2, \quad c_n^{12} = c_n^{21} = -n - k_0^2 n^3, \quad c_{mn}^{22} = 1 + k_0^2 n^4, \quad \gamma = \hat{c}_s^{-1}. \tag{36}$$

Eqs. (34) and (35) are complemented by the zero initial conditions for v_n, w_n, and their first derivatives.

The system (34) and (35) was approached numerically using finite differences. The second derivatives were approximated using central differences, and the integral term was approximated using the trapezoidal rule. The reason for choosing such a simple scheme is due to the fact that the systems are ordinary: the computational time is not an issue here, and the step size can be decreased almost indefinitely (or at least by as much as is needed to ensure that the scheme is well-converged). The approximation described results in the following finite-difference scheme (its convergence is addressed in Part II):

$$v_n^{i+1} = 2v_n^i - v_n^{i-1} - \frac{h^2}{\gamma^2}\{c_n^{11} v_n^i + c_n^{12} w_n^i\}, \tag{37}$$

$$w_n^{i+1} = 2w_n^i - w_n^{i-1} + \frac{2h^2}{\delta_h h + 2\gamma^2}\{\delta_h(p_n^i - hJ_n^i) - c_n^{21} v_n^i - c_n^{22} w_n^i\}, \tag{38}$$

where $\gamma = c_f/c_s$, $\delta_h = \rho_f \gamma^2 r_0 (\rho_s h_0)^{-1}$, h is the time step, and

$$J_n^i = \sum_{j=1}^{i-1} \{w_n^{j+1} - 2w_n^j + w_n^{j-1}\} h^{-2} \psi_n^{i-j}. \tag{39}$$

The resulting displacements were coupled with the analytical solution obtained for the radiation pressure, and the entire radiated field was simulated. We mention that even though the methodology used resulted in a semi-analytical solution of the problem, a completely analytical solution is possible as well. However, as discussed in Iakovlev (2006), the semi-analytical approach is far superior in terms of both its computational attractiveness and its suitability for extensive numerical simulations when a number of different shells need to be analysed.

We mention that the terms in the shell equations (2) and (3) multiplied by k_0^2 represent the bending stiffness. It was demonstrated in Iakovlev (2007) for the case of a submerged fluid-filled shell that, if the shell is very thin (i.e., if its thickness-to-radius ratio does not exceed 0.01), neglecting those terms does not result in qualitatively significant change in the acoustic field. There is no reason to believe that the present situation is any different in that context, but for the sake of completeness, we first carry out the simulations using the complete formulation that includes the bending stiffness, and then, in Part II, compare them to the results produced by the model where the bending stiffness is neglected.

5. Results and discussion

We analyse a steel shell with $\rho_s = 7800\,\mathrm{kg/m^3}$, $c_s = 5000\,\mathrm{m/s}$, $\nu = 0.30$, and the thickness-to-radius ratio $h_0/r_0 = 0.01$, where $r_0 = 1\,\mathrm{m}$ and $h_0 = 0.01\,\mathrm{m}$. The shell is submerged into water, $\rho_f = 1000\,\mathrm{kg/m^3}$ and $c_f = 1400\,\mathrm{m/s}$. Unless stated otherwise, we consider a cylindrical incident shock wave. For the reasons discussed in detail in Iakovlev (2006), we only consider a shock wave with a large stand-off S_R (the distance between the shell and the wave source), and assume it to be equal to four radii of the shell. The peak pressure in the front of the shock wave, p_α, and the exponential decay constant, λ, are assumed to be 250 kPa and 0.0001314 s, respectively. When discussing the numerical aspects of the solution, and also when introducing one-dimensional graphs specifically intended for use as benchmarks, we consider a plane shock wave. We do so for the reasons outlined in Appendix, and also because the plane wave was considered in Geers (1969), the work that largely inspired the present study. The plane wave is assumed to have the same parameters as the cylindrical one. We continue to use the terminology introduced in Iakovlev (2006), and refer to the points $\theta = 0$ and π as the 'head point' and 'tail point', respectively.

5.1. Diffraction

The diffraction of a shock wave on a rigid cylinder is, probably, one of the most well-studied shock reflection phenomena. A large number of high-quality experimental photographs are available, along with extensive numerical simulations utilizing a variety of models and techniques. It therefore appears worthwhile to consider the diffraction separately.

Fig. 2 shows the diffraction of the 'default' large stand-off shock wave on an absolutely rigid cylinder (certain low-magnitude non-physical numerical effects discussed in Appendix were eliminated in the shadow zone in a number of frames; the pressure range shown is not the same for all frames). The dynamics of the diffraction process follows the classical pattern where a Mach reflection develops. The Mach stems, as well as the triple points, can be easily identified during the later stages of the interaction. The Mach stems reach the tail point considerably later than the incident wave would have in the absence of the shell (2.74 versus 2.00), merge there, and start to propagate upstream. The pressure on the shell surface during this relatively late interaction is considerably lower than in the beginning of the process, but still is high enough to be taken into account when shock-subjected structures are analysed. During the late interaction, the Mach stems continue to travel upstream while the associated pressure is decaying. Overall, the diffraction process in the present, external case is much simpler and easier to analyse than in the case of an internal shock wave reflecting from the rigid walls of a cylindrical cavity.

We now turn to comparison of the present numerical results with the available experimental data. Surprisingly enough, experimental images depicting pressure fields induced by the interaction between very weak shock waves and/or non-stationary acoustic pulses and rigid cylinders are somewhat limited. It appears that the study by Ahyi et al. (1998), in which a cylindrical shell subjected to an acoustical pulse is considered, is the best reference available for such interaction [along with some additional experimental images, Ahyi (2006)]. Even though the acoustic field depicted in

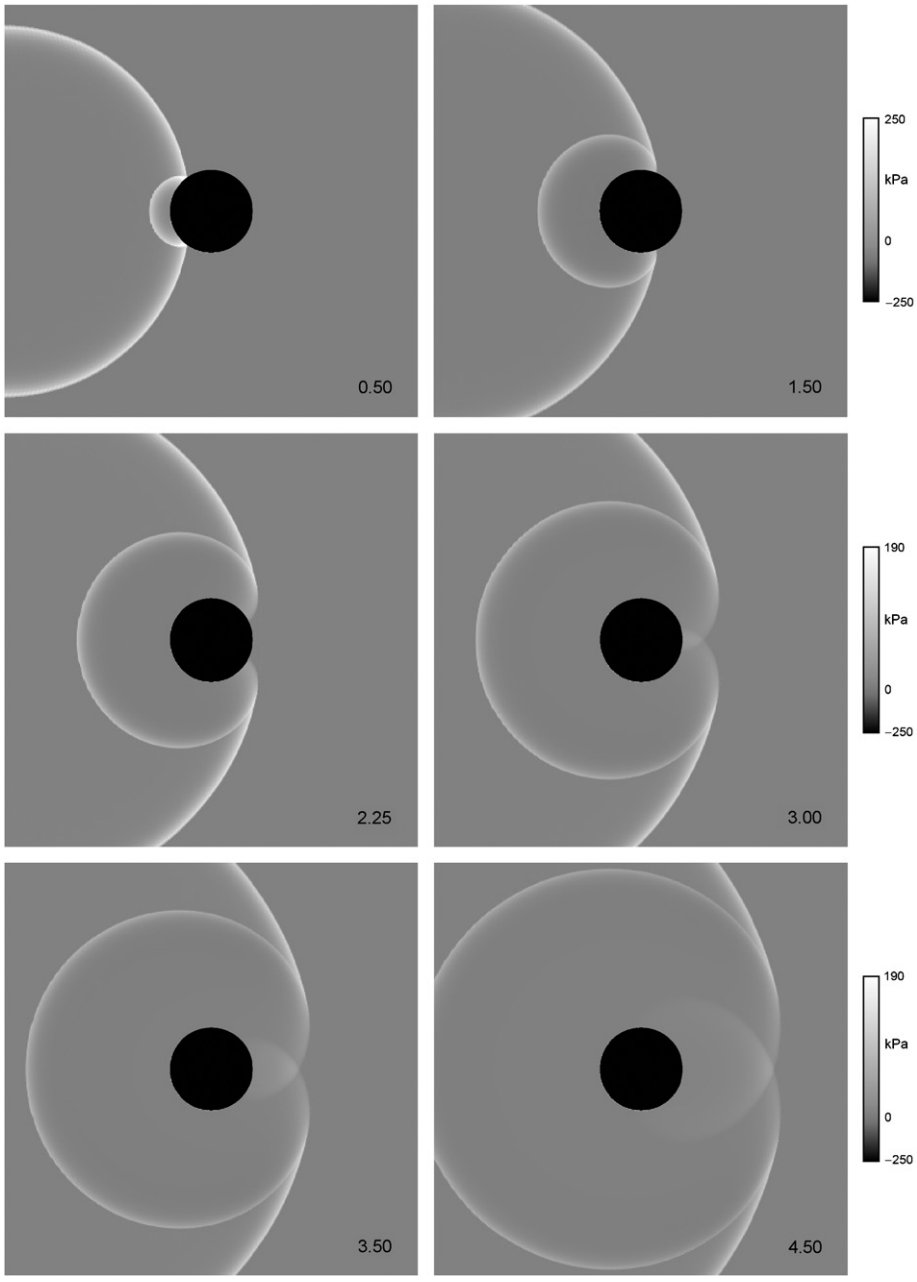

Fig. 2. Dynamics of the diffracted field.

those images is considerably more complex than the one observed for a rigid cylinder, the scattered wave is clearly identifiable, so the images can be successfully used for the analysis of the diffracted field.

Fig. 3(a) shows the total diffraction–radiation field induced by a very short acoustic pulse on a submerged cylindrical shell with the thickness-to-radius ratio of 0.06. Of the several different waves visible in the photograph, for now we shall only focus on the incident and diffracted waves labelled 'I' and 'SR', respectively; this means that we are only considering the waves induced by a shell as a 'rigid obstacle', and therefore its thickness is irrelevant. Even though the image is slightly clipped, most of the wave pattern of interest is still visible. Fig. 3(b) shows the numerically simulated diffraction field around a rigid cylinder subjected to a similar acoustic pulse. The 'absolute rigidity' of the cylinder is

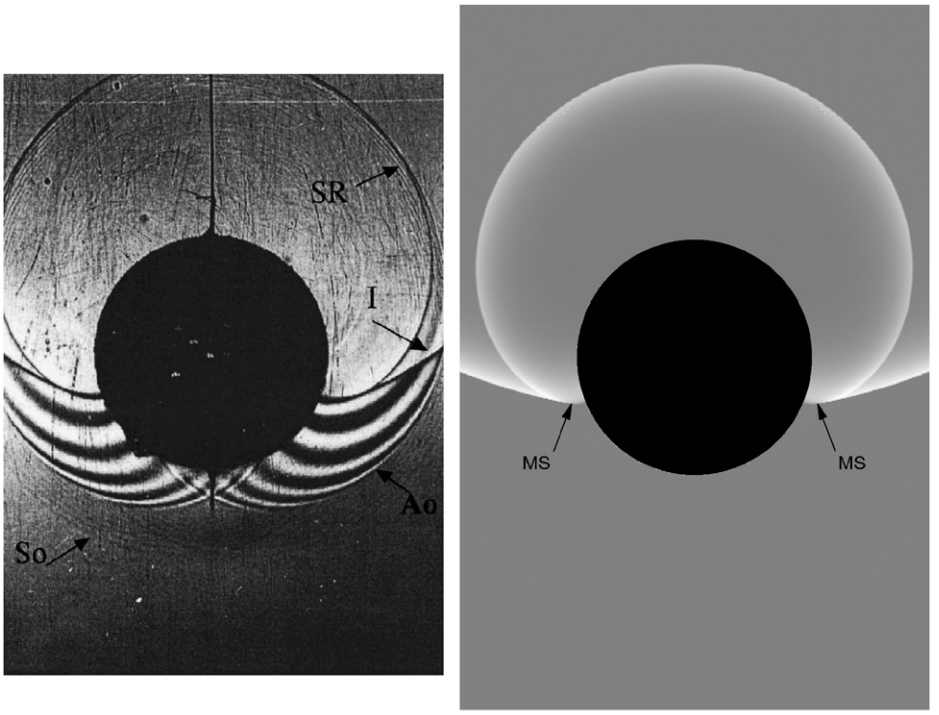

Fig. 3. Comparison of a numerically simulated diffracted field around an absolutely rigid cylinder, (b), to an experimental shadowgraph showing the acoustic field around a submerged empty shell induced by a similar shock wave, (a); $t = 1.50$ [Shadowgraph (a) is reprinted with permission from Ahyi et al. (1998), Figure 6(b), ©American Institute of Physics].

assumed, i.e. the only structure-induced wave observed is the diffracted one (in any real system, other types of waves would be detected around an elastic body, e.g., a compressional through wave). We also note that the wave source in the experiment appears to be closer to the shell than that in the simulated image, but that is not particularly important for the purposes of verifying the solution. As far as the scattered wave is concerned, the images evidently are in a very good agreement. In particular, such an important feature of the diffraction as the Mach stems is clearly identifiable in the simulated images (labelled 'MS'). We can therefore conclude that the solution obtained for the diffraction pressure appears to be adequately representing the actual diffracted field. We can also conclude that the linear model employed, in spite of its limitations, is quite suitable for analysis of the diffraction of very weak shock waves and acoustic pulses.

We note that Neubauer (1968a, b) studied the interaction of acoustic pulses with solid aluminium cylinders in water, and presented a considerable number of schlieren photographs of the interaction. Neubauer and Dragonette (1970) considered both solid cylinders and shells, and presented extensive visualizations of the interaction as well. However, almost all of the images included in the papers noted were for partial insonification, either by a narrow ray at a certain angular incidence or by a plane acoustic pulse incident on a quadrant of the cylinder, not the entire half of it; the only image of the full-cylinder insonification is similar to the images by Ahyi et al. (1998), but is of somewhat lower quality. The present approach can be used to simulate such partial insonification as well, but the solution would have to be modified to account for the fact that the acoustic pulse is non-symmetric. Such a modification can be easily accomplished by considering sin–cos series for the pressure and displacements instead of cos-only (or sin-only) series. The analysis of such interaction, however, is not an objective of the present work.

5.2. *Complete diffraction–radiation analysis*

Having established a good agreement between the simulated and experimentally observed diffracted fields, we move on to a considerably more interesting study, i.e. the complete diffraction–radiation analysis of the acoustic field induced by a shock-responding submerged shell. We note that the dynamics of the acoustic field in the present case is significantly less complex than that in the case of a fluid-filled shell (Iakovlev, 2006, 2007): all the most interesting wave

phenomena observed in that case, such as the reflection and focusing of the internal pressure wave, as well as the particularly complex multiple regular reflection that developed during the late interaction, took place in the internal fluid. In the present case, the variety of the wave reflection phenomena is quite limited, and the observed wave patterns are much easier to interpret.

Before we proceed to the analysis of the acoustic field, we note an important feature of the total diffracted–radiated field. Due to the fact that the structure is now elastic, it is capable of conveying elastic waves at the speed equal to that of the acoustic speed of the shell's material. Such waves, once induced at the point of contact between the shell and incident load, start to radiate into the fluid as they propagate circumferentially in the shell. Due to having the velocity of propagation that is supersonic relative to the surrounding fluid, the elastic waves induce an acoustic field that is registered quite far ahead of the incident and scattered waves (even though, once the waves are radiated into the fluid, they propagate at the same speed as the incident and diffracted ones). Due to this rather unique feature of the shell-radiated waves described, it appears reasonable to distinguish them from all other waves observed in the system; we shall refer to them as 'shell-induced waves'. We note that the magnitude of these waves is much lower than that of the incident and scattered waves. Nevertheless, they are an essential part of any shell–shock interaction.

We also mention another feature of the acoustic field around a submerged shell that makes visualizing the interaction more challenging than was the case when the internal field in a fluid-filled shell was considered. Namely, even though in both cases the shell-induced pressure is low-magnitude, it is negative in the internal fluid, while the (high-magnitude) pressure in the internal shock wave is positive. It, therefore, was very easy to visualize the dynamics of all the components of the total acoustic field using the same set of frames: if colour is used and the greens correspond to zero pressure, the yellows and reds to positive one, and the blues are used to display negative pressure, the shell-induced wave is always depicted by the tones of blue [e.g., Iakovlev (2007)], or, in halftone images, by the darker grays [e.g., Iakovlev (2006)]. In the present case, the pressure in the shell-induced waves is positive, as is the scattered one. Thus, if the latter is shown in full detail, either in colour or halftones, the former only appears as a scarcely visible wave feature. It is therefore necessary to consider two different series of plots: one where the high-magnitude components are depicted in detail at the expense of the low-magnitude features, and the other where the shell-induced waves are shown fully at the expense of the high-magnitude components. Even though the latter plots do not appear to be particularly realistic for the fact that the high-magnitude pressure has to be cut off at a certain threshold, they are nevertheless very informative. Since the propagation of the shell-induced waves has little to do with the propagation of the incident wave, it does not need to be shown in the low-magnitude plots.

We note that the practical relevance of the two types of plots is quite different. The high-magnitude ones are useful for estimating the peak pressure around the structure, as well as for the analysis of the contribution of the radiation pressure into the total acoustic field. The low-magnitude plots are not particularly useful when it comes to estimating the maximum pressure; however, they are critical to understanding the finer features of the interaction, specifically the response of the surrounding fluid to the dynamic behaviour of the shell as an elastic medium.

Fig. 4 shows the total acoustic field around a submerged elastic shell for the same instants as Fig. 2; the entire pressure range is shown. First of all, we notice that even though during the early and mid-interaction the geometry of the total field is the same as that of the diffracted field alone, the pressure decay behind the front of the scattered wave is considerably more intense than in the case of a rigid cylinder. This is a well-known fact [e.g., Wardlaw and Luton (2000), figure 8], but it certainly is comforting to observe it using the present, rather simple linear model [in fact, even though Wardlaw and Luton (2000) addressed an internal explosion in a cylindrical shell, the initial portions of the surface pressure time-histories are closely resembling the graphs in Fig. 5 to be discussed shortly].

From the practical point of view, the difference in the intensity of pressure decay becomes a particularly significant issue when secondary structures are placed around the primary shock-responding one, and the peak loads and/or impulses experienced by those need to be estimated. As we have just seen, using the diffraction pressure alone for such estimates will lead to a considerable overestimation of the impact of the scattered wave. Specifically, Fig. 5 shows the pressure time-histories at the surface (the head point, $\theta = 0$ and $r = 1.0$) and inside the fluid ($\theta = 0$ and $r = 1.5$); the total pressure for the case of a rigid cylinder is compared to that observed for an elastic shell (the numerical noise due to series convergence issues was filtered out from some parts of the graphs, see Part II). One can observe that the rates of decay behind the fronts of the diffracted and complete diffracted–radiated waves are dramatically different, and that the difference is particularly pronounced inside the fluid domain.

Namely, if we were to define the measure of the impact that a scattered wave has on a secondary structure as the integral of the pressure over the time interval corresponding to the first positive pressure peak in the scattered wave (a definition analogous to that of the impulse of a force), then, in the case considered, the impact of the diffracted–radiated wave on a secondary structure placed on or near the shell surface would be almost four times lower than that of the diffracted wave when the effects of the shell's elasticity are neglected; the same impact would be more than seven times lower when the structure is placed inside the fluid domain. We can therefore conclude that thin-walled elastic structures

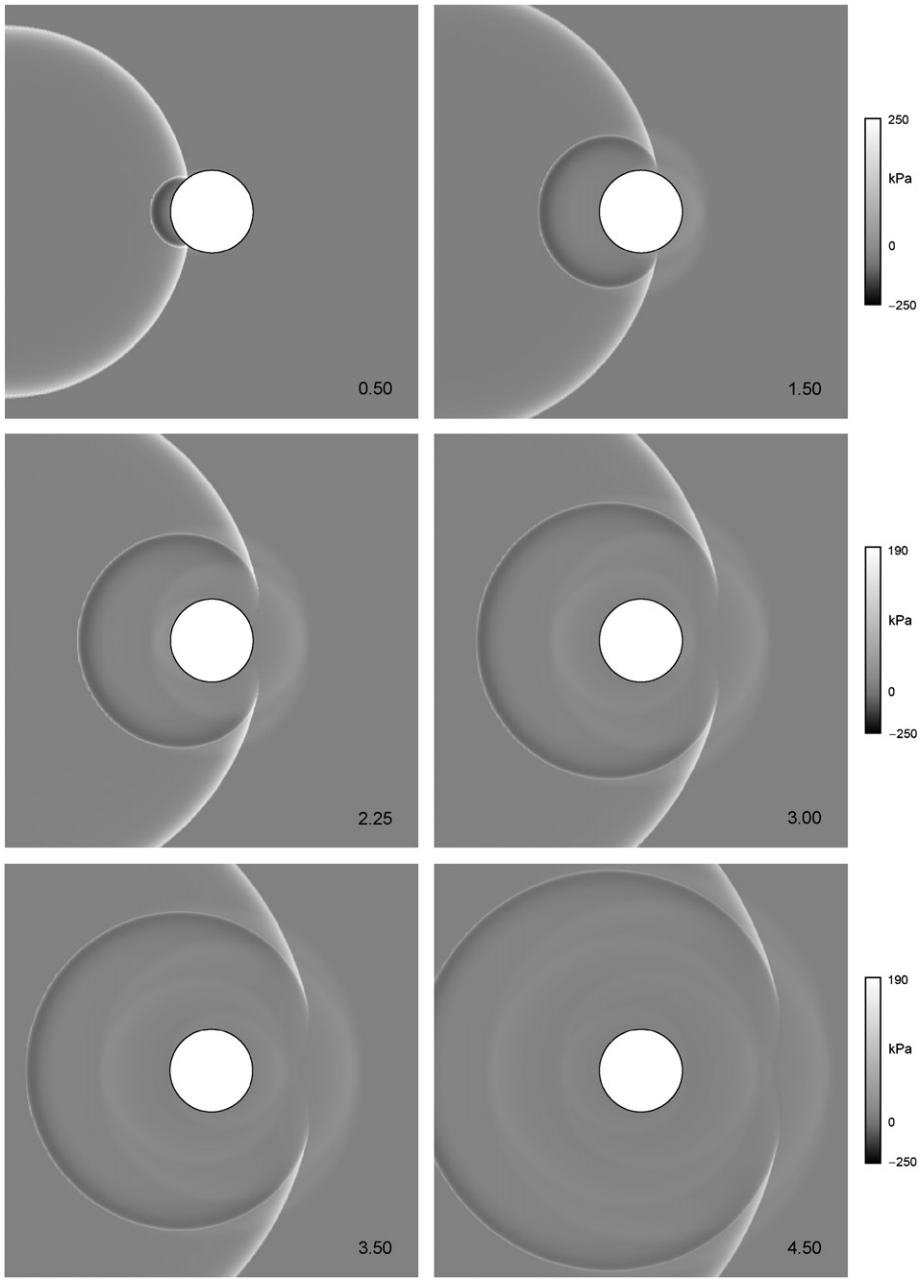

Fig. 4. Dynamics of the complete diffracted–radiated field around an empty submerged shell.

produce a much less destructive scattered field than rigid ones (here, of course, we assume that the loading is such that no non-linear effects take place, particularly cavitation and/or interaction with the explosion products). It may be beneficial to take this observation into consideration when designing industrial structures that are subjected to repeated shock loads: choosing thin-walled structures over solid ones may reduce overall destructive shock effects experienced by a multi-element installation.

We also note that, unlike in the case of a rigid cylinder, rather significant negative pressure is observed around an elastic shell, especially inside the fluid domain. This means that cavitation is a possibility for intense enough incident loads [e.g., Makinen (1998), Wardlaw and Luton (2000), and Mair (1999a)]. If cavitation does develop, the subsequent

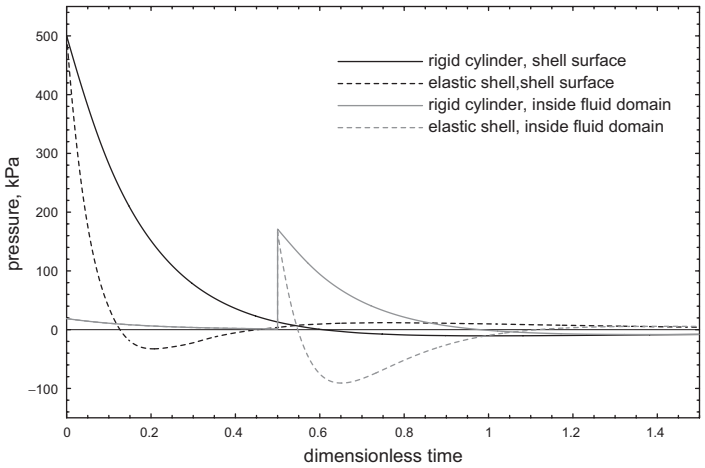

Fig. 5. Pressure time-history on the surface of the shell (head point, $r = 1.0$ and $\theta = 0$) and inside the fluid domain ($r = 1.5$ and $\theta = 0$) for an absolutely rigid cylinder (diffraction only) and an elastic shell (diffraction–radiation).

collapse of the cavitation region or/and separation of the shell from the fluid, both often leading to significant reloading of the shell, will considerably change the overall dynamics of the process. Of course, the present linear model will not be suitable for studying such complex, essentially non-linear phenomena. It, however, can certainly be used to give a preliminary idea about where cavitation is likely to develop, at least at the beginning of the interaction, and to hypothesize about the likeliest cavitation scenario to occur [a study similar to the one found in Iakovlev (2007)].

In the present case, it appears that the likeliest possibility is cavitation developing in a region adjacent to the shell surface early in the interaction (the low pressure zone in the snapshots for $t = 0.50$, Fig. 4). Such cavitation scenario will likely lead to separation of the fluid from the shell with its subsequent reloading [specific details on want happens when such separation occurs can be found in Wardlaw and Luton (2000)], and the rest of the process will be quite different from what is predicted by a linear model (or, for that matter, any other model that does not take cavitation into account). In particular, that means that the relatively narrow but extensive regions of negative pressure seen later in the interaction inside the fluid domain (which, if considered in isolation, may produce cavitation as well) may not be observed after cavitation takes place near the shell surface earlier in the process. Further discussion of the issue is beyond the scope of this work, and would require a much more sophisticated model and/or experiments.

Another interesting feature of the total field is that during the late interaction, the diffraction termination effects at the tail point at $t \approx 2.74$ (i.e. the merger of the Mach stems and their subsequent propagation upstream) are not clearly detectable. Again, this happens due to the presence of the negative pressure zone behind the front of the scattered wave which superposes with the positive pressure in the Mach stems. The result is that the Mach stems appear to terminate inside the fluid, without reaching the shell.

We now turn to the analysis of the shell-induced field, and first briefly summarize the dynamics of the elastic process in the shell that induces it. After the elastic wave is originated at the head point at the very beginning of the interaction, it propagates circumferentially around the shell with the dimensionless velocity given by c_s/c_f, or 3.57 in the present case, and reaches the tail point at $t \approx 0.88$. At that instant, the two waves propagating in the upper and lower halves of the shell superpose at the tail point causing a peak of the strain, and then continue to travel upstream. The propagation of the elastic waves, as well as their superposition, is accompanied by the constant radiation of pressure waves into the fluid. The surface of the shell moves outward, thus the shell-induced pressure is positive. The process is repeated with alternating superpositions at the head ($t \approx 1.76, 3.52, \ldots$) and tail ($t \approx 2.64, 4.40, \ldots$) points. We note that a brief analysis of the external radiated field was attempted in Iakovlev (2007), but only the surface pressure was addressed. Even though that allowed for general understanding of the external radiation, it was not entirely clear what happened in the fluid which is not in the immediate contact with the shell. That drawback is eliminated in the present work.

We first analyse Fig. 6 which shows the fully developed shell-induced wave system during the late interaction ($t = 4.50$, or more than twice the time it takes for the incident wave to move over the shell; the front of the incident wave is only shown schematically to ensure that other, lower-magnitude features of the field are obscured as little as possible). Recalling the mentioned timing of the superpositions of the elastic waves travelling in the shell, it is very easy to identify individual components of what appears to be a complex wave pattern. Five superpositions occur prior to the instant

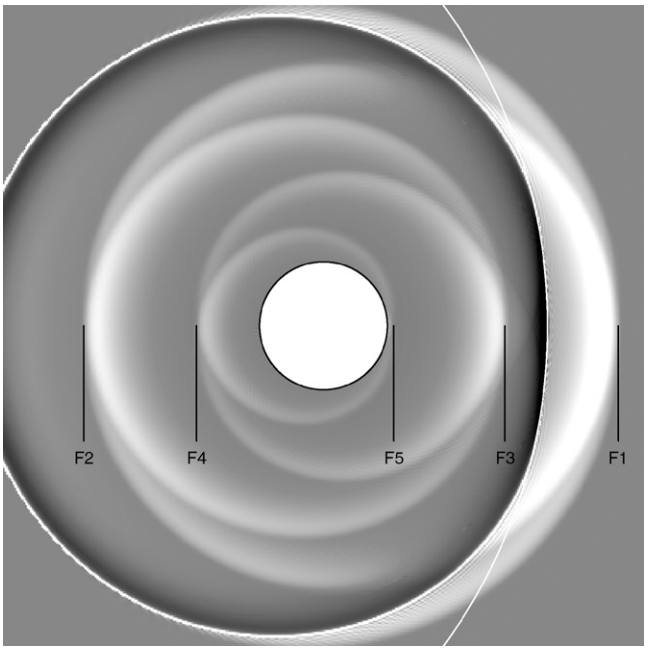

Fig. 6. Fully developed radiated (shell-induced) wave system during the late interaction, $t = 4.50$.

depicted, and all of them contribute to the acoustic field. The foremost points of the fronts of the respective radiated waves are labelled 'F1', 'F2', 'F3', 'F4', and 'F5', which correspond to the superposition times 0.88, 1.76, 2.64, 3.52, and 4.40, respectively.

We note that, even though the elastic waves in the shell travel at a supersonic (relative to the fluid) speed, the radiated waves themselves do not. As a result, only one shell-induced wave, F1, travels in front of the incident wave, with a constant backlog of about 1.1. This is a rather interesting result for the applications where the 'response time' is important, i.e. where the possibility of the arrival of a 'signal' to a certain point earlier than is expected based on the acoustical properties of the fluid is of significance. We also note that even though the same superpositions of the elastic waves occur in the case of a fluid-filled shell, the wave patterns in that case are considerably more complex due to the multiple reflections of the waves from the internal surface of the shell, and it is much harder to identify the individual components of the fully developed wave pattern using only one snapshot.

Having gained the understanding of what the shell-induced field is contributed by, we turn to the analysis of its dynamics, Fig. 7, which shows the formation and development of the wave pattern seen in Fig. 6. The entire process of the circumferential propagation and superposition of the shell-borne elastic waves, as well as their radiation into the fluid, are particularly easy to understand now. Along with Fig. 6, these plots are a very informative complement to the two-dimensional time–space images of the external pressure on the shell surface, as well as those of the strain in the shell, Iakovlev (2007, figures 11 and 12 (b)). We note that the high-frequency low-magnitude wave detectable just ahead of the scattered wavefront in Fig. 6, and also scarcely noticeable in the snapshots of Fig. 7, is another very interesting feature of an elastic shell–shock interaction. The origins and significance of this wave are addressed in detail in Part II.

6. Conclusions

The interaction between a submerged evacuated cylindrical shell and an external shock wave was considered. A two-dimensional simplification of the problem was formulated, and the validity and limitations of such a simplification were discussed. A semi-analytical solution of the problem was obtained, and the hydrodynamic field around the structure was simulated and analysed.

The diffraction of a shock wave on a rigid cylinder was addressed, and the dynamics of the corresponding acoustic field was visualized. All the classical features of the diffraction, such as the Mach stems and their propagation upstream

after the termination of the diffraction at the tail point, were observed. Two different incident waves were considered, a plane one and a cylindrical one, and their limitations and advantages were discussed.

Through comparison with experimental results for the diffraction, it was established that as long as the loading is limited to acoustic pulses and very weak shock waves, the linear model of the interaction, in spite of its relative simplicity, is adequate and captures all the important features of the process very well. Similar observation was made for a submerged fluid-filled shell (Iakovlev, 2006, 2007), and the good agreement with the experiments observed in the present work is a further indication of the suitability of the approach developed in the author's recent publications for modelling shell–shock interaction.

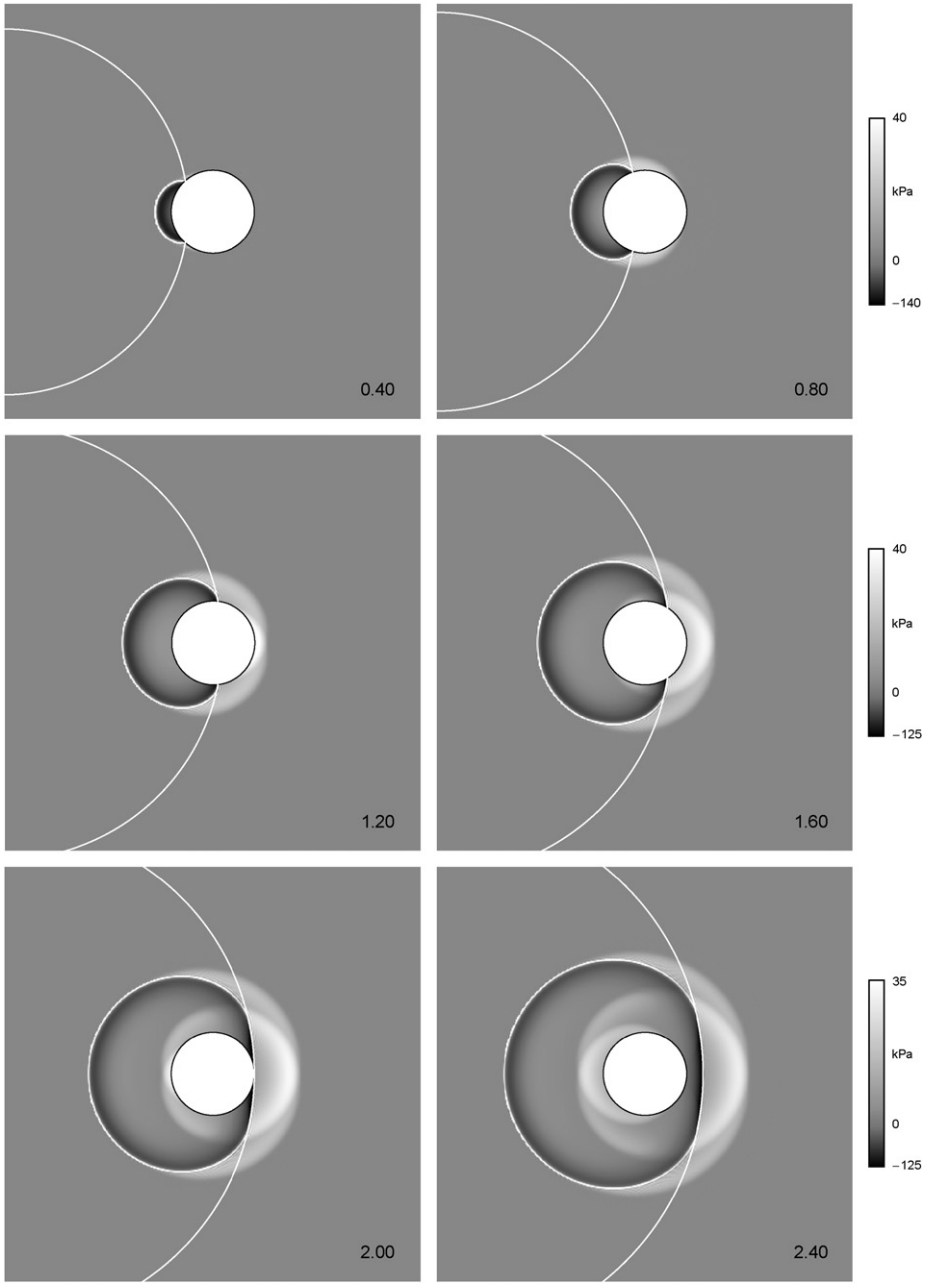

Fig. 7. Dynamics of the low-magnitude shell-induced field.

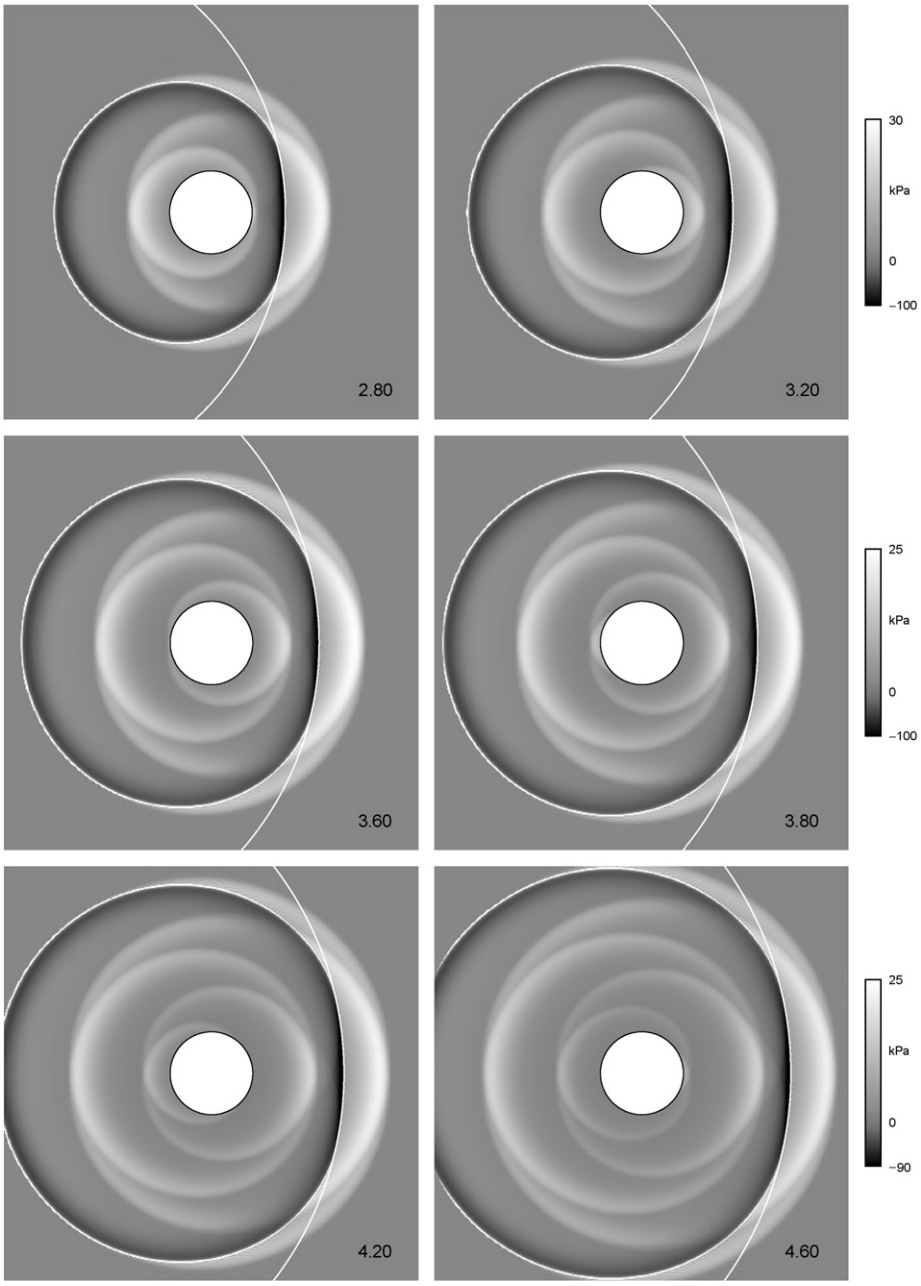

Fig. 7. (*Continued*)

The acoustic field around an elastic shell was addressed as well, and both the scattering and radiation by the shell were considered. The complete diffracted–radiated field was observed to be comprised of two components, the high-magnitude scattered one and the low-magnitude shell-induced one, the latter representing the radiation by the elastic waves propagating in the shell. The analysis of the high- and low-magnitude components was carried out separately, and the fully developed radiated wave system was addressed in detail. It was demonstrated that in the present case of an empty shell, it is quite easy to identify the components of the radiated field that are induced by the elastic waves on their multiple passages around the shell, even very late in the interaction.

The contribution of the radiation pressure into the total acoustic field was studied as well, and it was observed that the pressure decay behind the front of the wave scattered by an elastic shell is much more intense than that in the case of

a rigid cylinder. Even though a well-known fact, such analysis allowed to quantify the pressure difference for the particular case addressed. Specifically, it allowed for a preliminary estimation of the impulse experienced by secondary structures placed around the primary shock-responding one, and it appears that the adverse effects of shock loading on the secondary structures can be far more severe when the primary structure is rigid than when it is resilient, especially inside the fluid domain.

The possibility of cavitation in the system was briefly discussed as well, based on the conclusions drawn from the results produced by the present model. The fluid around the elastic shell was observed to be much likelier to experience cavitation than that around a rigid cylinder, and it appeared that the likeliest cavitation scenario is that when the separation of the shell and fluid occurs, followed by the cavitation region collapse and subsequent reloading of the structure.

From the historical perspective, the present work is an extension of an analytical solution introduced several decades ago (Geers, 1969) to a point where it can be used to simulate the two-dimensional interaction, not only the one-dimensional distribution of the pressure on the shell surface. Numerical analysis of the solution, as well as a discussion of certain theoretical issues and further comparison with experimental data, are the subject of Part II.

Acknowledgements

The author gratefully acknowledges the financial support of the Natural Sciences and Engineering Research Council (NSERC) of Canada (Discovery Grant 261949), the Killam Trusts, and the Faculty of Engineering, Dalhousie University. The author is also grateful to Dr Ayayi Claude Ahyi of the Auburn University, Alabama, USA, for granting a permission to reproduce photographs from one of his publications, and for sharing a previously unpublished experimental image that was helpful in validating some of the numerical simulations presented in this paper. Last but not least, the author thanks Ryan Barnes, a Mechanical Engineering student at Dalhousie University, for his dedicated assistance with often challenging numerical analysis that ensured the accuracy of the results presented.

Appendix A. Remarks on the choice of the incident wave

When a three-dimensional interaction is considered, the choice of the incident wave is not an issue: within the realms of the linear approach, a spherical shock wave with the exponential pressure decay behind the front [e.g., Cole (1948)] is known to be a reasonably adequate model of the actual incident shock wave generated as a result of a relatively distant explosion. A plane shock wave with the exponential pressure decay is another possibility which, perhaps, is of lesser practical value since it is only suitable when the distance between the source of the wave and the shell is very large. One might expect that in the two-dimensional case the situation is similar. To some extent, this is true; there are, however, certain issues that one faces when dealing with a simplified two-dimensional formulation of the problem. Those issues are the subject of this appendix.

The pressure in a spherical shock wave with exponential pressure decay is given by (the dimensional form of the equations is used throughout this appendix; the derivation of the equation can be found in Iakovlev (2006))

$$p_0 = \frac{p_\alpha S_R}{R}\, \mathrm{e}^{-(\tau - c_f^{-1}(R-S_R))\lambda^{-1}}\, \mathrm{H}(\tau - c_f^{-1}(R-S_R)), \tag{40}$$

where

$$R = \sqrt{R_0^2 + x^2 + \varrho^2 - 2R_0\varrho\cos\theta}, \tag{41}$$

p_α is the pressure in the front of the wave when it first impinges on the shell, λ is the rate of exponential decay, $S_R = R_0 - r_0$ is the shock wave stand-off (the distance between the source and the shell), x is the axial coordinate of the respective cylindrical coordinate system, and H is the Heaviside unit step function. The incident potential is given by

$$\phi_0 = -\frac{\lambda p_\alpha S_R}{\rho_f R}\, \mathrm{e}^{-(\tau - c_f^{-1}(R-S_R))\lambda^{-1}}\, \mathrm{H}(\tau - c_f^{-1}(R-S_R)). \tag{42}$$

If we want to reduce the problem to its two-dimensional counterpart and only address the middle cross-section of the shell, but, at the same time, wish to retain as much of the problem's geometry as possible, we would have to assume that there is no change associated with the axial coordinate, and to consider a 'cylindrical extension' of what is observed in the middle cross-section. That, in particular, would imply that we would have to consider the 'middle cross-section' of

the three-dimensional spherical wave as the incident load; more specifically, the 'cylindrical extension' of the pressure observed in the middle cross-section would have to be addressed. The pressure in such a wave would still be given by (40), but the radial distance would be different, i.e. we would have

$$p_0 = \frac{p_\alpha S_R}{R^*} \mathrm{e}^{-(\tau - c_f^{-1}(R^* - S_R))\lambda^{-1}} \mathrm{H}(\tau - c_f^{-1}(R^* - S_R)), \tag{43}$$

where

$$R^* = \sqrt{R_0^2 + \varrho^2 - 2R_0\varrho\cos\theta} \tag{44}$$

and

$$\phi_0 = -\frac{\lambda p_\alpha S_R}{\rho_f R^*} \mathrm{e}^{-(\tau - c_f^{-1}(R^* - S_R))\lambda^{-1}} \mathrm{H}(\tau - c_f^{-1}(R^* - S_R)). \tag{45}$$

Such transition from a complete three-dimensional model to a simplified two-dimensional one has been carried out in Iakovlev (2006, 2007), and it has been demonstrated that the results obtained using the latter were qualitatively very similar to those observed in the middle cross-section of a three-dimensional shell subjected to a spherical shock wave (assuming that the parameters of the waves did not change). It was therefore concluded that, for practical purposes, a two-dimensional simplification of the three-dimensional spherical shock wave (referred here as a 'cylindrical incident wave') was an acceptable trade-off, at least when one is primarily concerned with the middle cross-section of the shell: both the complexity of the model and computational time were reduced dramatically, without compromising the qualitative validity of the results.

Unfortunately, such transition from three to two dimensions gives rise to a rather serious theoretical issue that may not be immediately apparent. Namely, in three dimensions, both spherical (produced by a point source) and plane waves can have an arbitrary functional form [e.g., Courant and Hilbert (1962), pp. 188 and 196], and, therefore, it is possible to easily model an exponential (or any other, for that matter) decay. In two dimensions, however, a shock wave produced by a point source, or a so called cylindrical wave, cannot have an arbitrary functional form [Courant and Hilbert (1962), pp. 194 and 196], and one faces difficulties when modelling an exponential decay using such a wave. Not less importantly, the equation for the potential in a cylindrical wave is not a two-dimensional reduction (accomplished by neglecting the axial dependence) of the equation for the potential in a spherical wave (which was assumed to be the case when a 'cylindrical incident wave' was introduced, compare Eqs. (40) and (43)).

Thus, even though the reduced two-dimensional version of the three-dimensional potential in a spherical shock wave was shown to be very suitable for a simplified (but, nevertheless, physically adequate) analysis of the interaction, it does not satisfy the two-dimensional wave equation for the potential ϕ_0

$$\frac{\partial^2\phi_0}{\partial\varrho^2} + \frac{1}{\varrho}\frac{\partial\phi_0}{\partial\varrho} + \frac{1}{\varrho^2}\frac{\partial^2\phi_0}{\partial\theta^2} = \frac{\partial^2\phi_0}{\partial\tau^2}. \tag{46}$$

This appears to be a very significant drawback of the model utilizing a 'cylindrical incident wave', and seems to compromise the validity of the results obtained using such a model. In the present case, however, no major physical discrepancies have been noticed, and a very good agreement with experiments has been observed (Iakovlev, 2006, 2007). Why? The reason for such physically adequate results is in the fact that even though the potential given by (45) does not satisfy the wave equation (46), the error over the entire time–space domain of interest is insignificant. The latter fact was established through numerical computations carried out over the entire r, θ, t domain. The numerical procedure used was first tested on a plane wave for which, expectedly, it produced the values that were very close to zero. For the cylindrical incident wave used in the present study, the error was observed to be usually very small, with the exception of relatively localized regions where it increased significantly but still was in the order of 5% of the maximum magnitude of the largest term(s) in (46).

However, since the error is not negligibly small, the solution obtained using the cylindrical incident wave exhibits certain non-physical effects. Even though the magnitude of those effects is very low, there are regions where the physical inconsistency is obvious. Specifically, it is most pronounced in the shadow zone at the times when the zone is still unaffected by the diffracted wave (and, therefore, the pressure there should be zero). Fig. 8 shows the diffracted field at $t = 2.40$ for (a) the plane (Eq. (47)) and (b) cylindrical incident waves with the same rate of exponential decay, $\lambda = 0.0001314$ s. Unlike in the main text on the paper, the halftones are assigned in such a way that even very small negative pressure becomes noticeable, thus making the discrepancies easy to detect; the overall images, of course, are

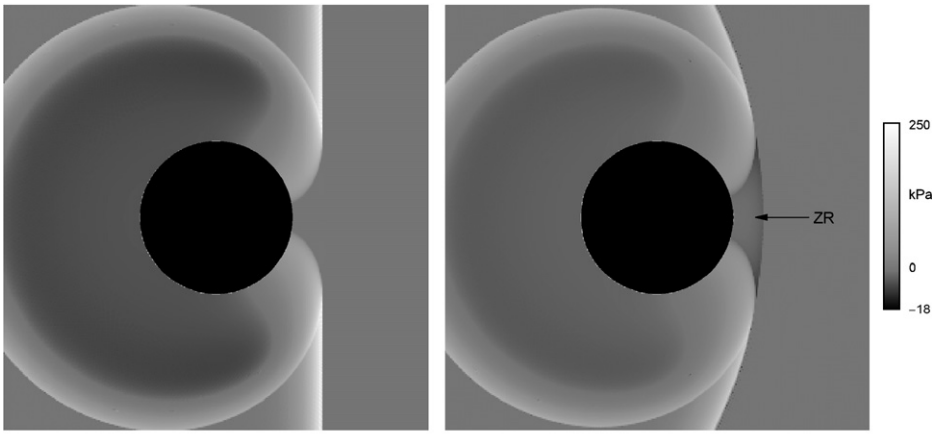

Fig. 8. Comparison of the diffraction fields induced around a rigid cylinder by (a) a plane, Eq. (47), and (b) cylindrical, Eq. (43), incident waves.

less realistic for such a choice of halftones. The pressure in a two-dimensional plane incident wave is given by

$$p_0 = p_\alpha \mathrm{e}^{-(\tau + c_f^{-1}(r\cos\theta - r_0))\lambda^{-1}} \mathrm{H}(\tau + c_f^{-1}(r\cos\theta - r_0)), \tag{47}$$

which can also be deduced from (43) if one assumes that $R_0 \to \infty$.

From the physics of the problem, we know that, for any incident wave, there is always a region in the shadow zone that is not affected by the diffracted wave at instants when, in the absence of the shell, the front of the incident wave would have already passed over the region in question. One can see that this is indeed so for the plane wave. In the case of the cylindrical incident wave, however, the pressure is no longer zero throughout the shadow region in question (labelled ZR). The non-zero pressure observed is definitely not physical, and is present due to the fact that the potential in the cylindrical incident wave does not satisfy the two-dimensional wave equation.

The mismatch illustrated appears to be the most noticeable discrepancy caused by the use of the two-dimensional simplification (43). Its magnitude does not exceed 3% of the global maximum of the diffraction pressure, and is small even relative to the local maximum (about 8% for the instant considered). We emphasize that when the acoustic fields are visualized in such a way that the halftones are distributed approximately equally between the positive and negative values of the pressure, the discrepancy in question is much less pronounced. It can also be easily eliminated altogether (as was done in the images in the main text).

In summary, the author feels that, in spite of the fact that the simplified two-dimensional version of the three-dimensional spherical wave does not satisfy the wave equation (and, as a result, produces non-physical effects), the advantages of using such a simplified model considerably outweigh its drawbacks. It produces the results that are close to what would be observed for a complete three-dimensional model, but requires an incomparably shorter computational time to do so. At the same time, the non-physical effects produced by the model are at most second-order.

References

Ahyi, A.C., Pernod, P., Gatti, O., Latard, V., Merlen, A., Uberall, H., 1998. Experimental demonstration of the pseudo-Rayleigh (A_0) wave. Journal of the Acoustical Society of America 104, 2727–2732.

Ahyi, A.C., 2006. Personal communication.

Bryson, A.E., Gross, R.W.F., 1961. Diffraction of strong shocks by cones, cylinders, and spheres. Journal of Fluid Mechanics 10, 1–16.

Cole, R.H., 1948. Underwater Explosions. Dover Publications, New York.

Courant, R., Hilbert, D., 1962. Methods of Mathematical Physics. Wiley, New York.

Drikakis, D., Ofengeim, D., Timofeev, E., Voionovich, P., 1997. Computation of non-stationary shock-wave/cylinder interaction using adaptive-grid methods. Journal of Fluids and Structures 11, 665–691.

Geers, T.L., 1969. Excitation of an elastic cylindrical shell by a transient acoustic wave. Journal of Applied Mechanics 36, 459–469.

Geers, T.L., 1972. Scattering of a transient acoustic wave by an elastic cylindrical shell. Journal of the Acoustical Society of America 51, 1640–1651.
Heilig, G., 1999. Shock-induced flow past cylinders with various radii. In: Proceedings of the 22nd International Symposium on Shock Waves, Imperial College, London, UK, pp. 1099–1104.
Heilig, W.H., 1969. Diffraction of a shock wave by a cylinder. Physics of Fluids 12 (Suppl. I), 154–157.
Huang, H., 1975. Scattering of spherical pressure pulses by a hard cylinder. Journal of the Acoustical Society of America 58, 310–317.
Huang, H., 1979. Transient response of two fluid-coupled cylindrical elastic shells to an incident pressure pulse. Journal of Applied Mechanics 46, 513–518.
Huang, H., Mair, H., 1996. Neoclassical solution of transient interaction of plane acoustic waves with a spherical elastic shell. Shock and Vibration 3, 85–98.
Huang, H., Wang, Y.F., 1970. Transient interaction of spherical acoustic waves and a cylindrical elastic shell. Journal of the Acoustical Society of America 48, 228–235.
Huang, H., Wang, Y.F., 1971. Early-times interaction of spherical acoustic waves and a cylindrical elastic shell. Journal of the Acoustical Society of America 50, 885–891.
Iakovlev, S., 2004. Influence of a rigid co-axial core on the stress–strain state of a submerged fluid-filled circular cylindrical shell subjected to a shock wave. Journal of Fluids and Structures 19, 957–984.
Iakovlev, S., 2006. External shock loading on a submerged fluid-filled cylindrical shell. Journal of Fluids and Structures 22, 997–1028.
Iakovlev, S., 2007. Submerged fluid-filled cylindrical shell subjected to a shock wave: fluid–structure interaction effects. Journal of Fluids and Structures 23, 117–142.
Junger, M.C., Feit, D., 1972. Sound, Structures, and their Interaction. MIT Press, Cambridge, USA.
Latard, V., Merlen, A., Preobazhenski, V., Ahyi, A.C., 1999. Acoustic scattering of impulsive geometrical waves by a glass sphere in water. Applied Physics Letters 74, 1919–1921.
Mair, H.U., 1999a. Review: hydrocodes for structural response to underwater explosions. Shock and Vibration 6, 81–96.
Mair, H.U., 1999b. Benchmarks for submerged structure response to underwater explosion. Shock and Vibration 6, 169–181.
Makinen, K., 1998. Cavitation models for structures excited by a plane shock wave. Journal of Fluids and Structures 12, 85–101.
Merlen, A., Pernod, P., Ahyi, A., Kemmou, A., 1995. Shock-wave diffraction by an elastic sphere in water. In: Proceedings of the 20th International Symposium on Shock Waves, vol. I, Pasadena, CA, USA, pp. 513–518.
Neubauer, W.G., 1968a. Experimental observation of three types of pulsed circumferential waves on solid aluminium cylinders. Journal of the Acoustical Society of America 44, 1150–1152.
Neubauer, W.G., 1968b. Pulsed circumferential waves on aluminium cylinders in water. Journal of the Acoustical Society of America 45, 1134–1144.
Neubauer, W.G., Dragonette, L.R., 1970. Observation of waves radiated from circular cylinders caused by an incident pulse. Journal of the Acoustical Society of America 48, 1135–1149.
Oakley, J.G., Puranik, B.P., Anderson, M.H., Peterson, R.R., Bonazza, R., Weaver, R.P., Gittings, M.L., 1999. An investigation of shock-cylinder interaction. In: Proceedings of the 22nd International Symposium on Shock Waves, Imperial College, London, UK, pp. 941–946.
Ofengeim, D.Kh., Drikakis, D., 1997. Simulation of blast wave propagation over a cylinder. Shock Waves 7, 305–317.
Sprague, M.A., Geers, T.L., 1999. Response of empty and fluid-filled, submerged spherical shells to plane and spherical, step-exponential acoustic waves. Shock and Vibration 6, 147–157.
Sun, M., 1998. Numerical and experimental studies of shock wave interaction with bodies. Ph.D. Thesis, Tohoku University, Japan.
Takano, Y., Hayashi, K., Goto, T., 1997. A computational procedure for interactions of shock waves with solid materials in liquid. In: Proceedings of the 21st International Symposium on Shock Waves, Great Keppel Island, Australia, pp. 1039–1044.
Voinovich, P., Merlen, A., Tomofeev, E., Takayama, K., 2001. Numerical simulation of wave scattering at shock-loaded metallic plates and shells in water. In: Proceedings of the 23rd International Symposium on Shock Waves, Fort Worth, TX, USA, pp. 954–963.
Wardlaw Jr., A.B., Luton, J.A., 2000. Fluid–structure interaction mechanisms for close-in explosions. Shock and Vibration 7, 265–275.
Yang, J.Y., Liu, Y., 1987. Computation of shock wave reflection by circular cylinders. AIAA Journal 25, 683–689.
Zhang, P., Geers, T.L., 1993. Excitation of a fluid-filled, submerged spherical shell by a transient acoustic wave. Journal of the Acoustical Society of America 93, 696–705.